Incidence Angle Optimization for Formation-Flying Across-Track SAR Interferometry

Riccardo Longari, Francesca Scala, Gabriella Gaias, Gerhard Krieger, *Fellow, IEEE*, and Michelangelo Villano, *Senior Member, IEEE*

Abstract—Single-pass across-track synthetic aperture radar (SAR) interferometry using formation flying is a well-established technique for the generation of high-quality digital elevation models (DEMs), as it avoids temporal decorrelation and allows for long baselines, thus leading to high height accuracy. A successful implementation, employed in the TanDEM-X mission, foresees the use of a Helix formation, which entails a reduced control effort to be maintained in the presence of external perturbations. However, an intrinsic limitation of the Helix concept lies in the inherently time-varying baseline and height of ambiguity (HoA), which results in non-homogeneous DEM performance. This letter proposes an analytical method to minimize the HoA variability at the global level by optimizing the range of incidence angles used at each latitude. The approach is primarily aimed at systems, such as TanDEM-X, for which the area to be imaged becomes significantly smaller than the ground access range as the latitude increases. A two-step approach is presented: An initial approximate solution is derived in closed form and subsequently refined. The method is validated against numerical results and compared with simpler strategies involving fixed incidence angles, showing reduced variation of the HoA for different formation parameters. The procedure presented in this work could enable a better operation of current interferometric SAR systems and foster an improved design of future ones.

Keywords – **Across-track interferometry, digital elevation model (DEM), formation flying, Helix formation, incidence angle, synthetic aperture radar (SAR), TanDEM-X.**

I. INTRODUCTION

SINGLE-PASS across-track synthetic aperture radar (SAR) interferometry employing formation flying is a powerful technique for the generation of high-quality digital elevation models (DEMs) [1]. Systems employing long across-track baselines can achieve unparalleled height accuracy: As an example, the TanDEM-X mission by the German Aerospace Center (DLR) has produced the most accurate high-resolution global DEM to date, achieving 2-m relative height accuracy for a posting of 12 m, leveraging baselines ranging from several hundred to over a thousand meters.

A successful implementation, employed by TanDEM-X and later on by the Chinese L-band SAR LuTan-1 mission, foresees the use of a Helix configuration, which combines the natural motion of the satellites with intrinsic passive safety, ensuring a more practical and economical management of the formation.

Despite this advantage, the Helix concept entails an inherently time-varying baseline, which leads to a corresponding variation of the height of ambiguity (HoA), the height over which the interferometric phase varies by 2π, resulting in non-uniform height accuracy over the imaged area. This becomes particularly critical for missions requiring global coverage, where it is desired to maintain uniform performance over a wide range of latitudes. Notably, the SAR acquisitions requirements change with latitude: Due to Earth's curvature, in fact, the width of the required ground coverage decreases moving towards the poles, as the ground access ranges of consecutive orbits increasingly overlap, reducing the area that has to be imaged, as sketched in Fig. 1.

Some SAR systems are particularly well-suited to exploit this effect, as they map in subsequent acquisitions multiple narrower swaths to cover a ground access range of considerable width. In TanDEM-X, for instance, a ground access range of 240 km is mapped during different orbits with swaths of about 30 km for the stripmap acquisition mode by selectively activating proper elevation beams, which point to different parts of the ground access range. For this kind of system, the problem of ensuring a uniform HoA can be partially addressed by a thoughtful choice of the non-overlapping portion of the ground access range at each latitude. This, in turn, can be equivalently formulated as the optimal selection of the corresponding range of incidence angles.

This work derives an analytical expression for the range of incidence angles that minimizes the variability of the HoA as a function of the latitude in the case of Helix formations.

R. Longari, G. Krieger, and M. Villano are with the German Aerospace Center (DLR), Microwaves and Radar Institute, 82234 Weßling, Germany (email: michelangelo.villano@dlr.de).

F. Scala is with Starion Group for ESA-ESTEC, 2201 AZ Noordwijk, Netherlands (email: francesca.scala@ext.esa.int).

G. Gaias is with Politecnico di Milano, Department of Aerospace Science and Technology, 20156, Milan, Italy (email: gabriella.gaias@polimi.it).
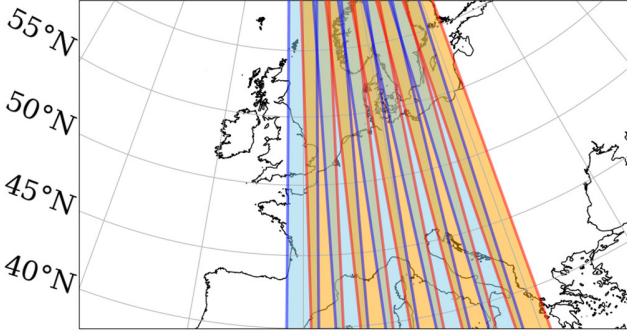
Fig. 1. Progressive overlapping of a 240 km-wide access range over ten consecutive orbits, displayed in alternating colors for latitude ranging from 40°N to 60°N, starting from Greenwich meridian.

II. Helix Formation Framework

The relative dynamics is formulated employing the relative eccentricity and inclination vectors $\mathbf{\Delta e}$ and $\mathbf{\Delta i}$ [2]:

$$\begin{cases} \mathbf{\Delta e} = \begin{bmatrix} e_c\cos\omega_c - e_d\cos\omega_d \\ e_c\sin\omega_c - e_d\sin\omega_d \end{bmatrix} = \delta e \begin{bmatrix} \cos\varphi \\ \sin\varphi \end{bmatrix} \\ \mathbf{\Delta i} = \begin{bmatrix} i_c - i_d \\ (\Omega_c - \Omega_d)\sin i \end{bmatrix} = \delta i \begin{bmatrix} \cos\vartheta \\ \sin\vartheta \end{bmatrix} \end{cases} \tag{1}$$

where δe and δi and φ and ϑ are the magnitudes and phases of $\mathbf{\Delta e}$ and $\mathbf{\Delta i}$, respectively, and the subscripts c and d indicate the chief and the deputy satellite, respectively. Additionally, e denotes the orbit's eccentricity, ω the argument of the perigee, i the inclination angle, and Ω the right ascension of the ascending node.

If the assumptions of the Hill-Clohessy-Wiltshire (HCW) equations hold, bounded, periodic orbits centered on the chief can be expressed using the amplitude-phase formulation of the relative eccentricity and inclination vectors:

$$\begin{cases} B_r(u) = -a\,\delta e \cos(u - \varphi) \\ B_{at}(u) = 2\,a\,\delta e \cos(u - \varphi) \\ B_{xt}(u) = a\,\delta i \sin(u - \vartheta) \end{cases} \tag{2}$$

where B_r, B_{at}, and B_{xt} are the radial, along-track, and across-track components of the baseline, respectively, a denotes the semi-major axis of the chief's orbit, and u stands for the mean argument of latitude, defined as the sum of the argument of the perigee and the mean anomaly. Under the assumption of pure Keplerian motion, u is the only term that varies with time.

In the following, we assume that the chief satellite flies in a circular and polar orbit. The circularity, already required by the HCW equations, implies that the mean and true arguments of latitude are identical; the polar hypothesis ensures that all latitudes are covered. These two assumptions allow us to consider u as equivalent to the geocentric latitude ϕ over which the satellites pass. In typical SAR missions, sun-synchronous orbits are often employed by imposing an inclination between 96° to 99° depending on the altitude, hence slightly deviating from a perfectly polar orbit. Indeed, the polar assumption, which we retain to display the results without neglecting any latitude value, could be easily relaxed by considering that u and ϕ are related by:

$$\sin\phi = \sin u \sin i. \tag{3}$$

For convenience in describing the relative motion, we will initially make use of the variable u instead of ϕ. Additionally, we will assume a spherical shape of the Earth, without distinguishing between geocentric and geodetic latitude. Moreover, the Earth rotation is not considered in this work.

As previously stated, we limit ourselves to considering Helix orbits, which are bounded orbits obtained after having imposed the condition $\vartheta = \varphi + k\pi$. This allows for maintaining a safe distance in the $B_r - B_{xt}$ plane, which is crucial considering the higher uncertainties the along-track component is subject to. In fact, this configuration ensures that the vertical coordinate is maximized when the across-track one reaches zero and vice versa [2]. Moreover, the phases of the relative eccentricity and inclination vectors (φ and ϑ) are often set equal to $\pi/2$ (or $3\pi/2$), like for TanDEM-X. This choice has the merit of providing a more robust stability to the perturbing effect of Earth's oblateness (J_2) because it eliminates the secular evolution of the $\mathbf{\Delta i}$ vector, leading to a less frequent request of a control action to maintain the safety of the formation as well as to a slower deviation from the nominal configuration [2]. We will adopt this assumption in the case studies presented in Section V.

III. Parametric Expression of the Height of Ambiguity

We consider the height of ambiguity as the figure of merit to optimize. Specifically, we focus on the bistatic case, where the HoA is defined as:

$$\text{HoA} = \frac{\lambda r_0(\theta_i)\sin\theta_i}{B_\perp(\theta_i, u)}, \tag{4}$$

where λ indicates the wavelength, r_0 the slant range, and $B_\perp$ the orthogonal baseline [1]. Please note that a height variation implies a proportional HoA variation, which justifies a spherical Earth assumption for low Earth orbit satellites. To understand how the angle of incidence θ_i influences the HoA, we need to explicit the relations between all quantities in (4).

Referring to the geometry on the left panel of Fig. 2, the position of a generic point on the ground can be defined by
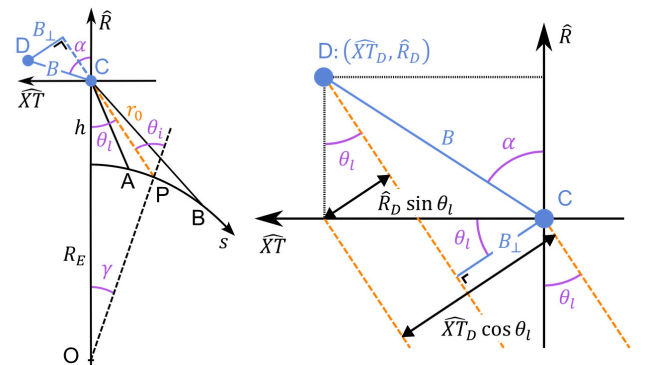

Fig 2. Sketch of the geometry in the radial-across-track plane. Left: angular and ground range coordinates definition. Right: relative geometry of chief and deputy satellites.

means of either the incidence angle θ_i or the look angle θ_l, whose relation is given by the law of sines [3]:

$$\sin\theta_i = \frac{R_E + h}{R_E}\sin\theta_l \, , \qquad (5)$$

where R_E is the radius of the Earth, or through the angle γ measured from the center of the Earth, as:

$$\theta_l = \theta_i - \gamma \, . \qquad (6)$$

The ground range coordinate of a generic point P is indicated as s_P and can be related to the corresponding look angle θ_{lP} using (5) and (6):

$$\tan\theta_{lP} = \frac{\sin\gamma_P}{\frac{R_E + h}{R_E} - \cos\gamma_P} = \frac{\sin\left(\frac{s_P}{R_E}\right)}{\frac{R_E + h}{R_E} - \cos\left(\frac{s_P}{R_E}\right)} \, . \qquad (7)$$

The width of the total ground width to be imaged for a given latitude $W_g(\phi)$ reads:

$$W_g(\phi) = s_B - s_A = W_{g0}\cos\phi, \qquad (8)$$

where W_{g0} is the ground access range at the equator.

The expression of r_0 as a function of the look angle can be computed by applying the law of cosines to the triangle OCP, from which the following expression is obtained:

$$r_0(\theta_l) = (R_E + h)\cos\theta_l - \sqrt{(R_E + h)^2\cos^2\theta_l - (h^2 + 2R_E h)} \qquad (9)$$

with θ_i (θ_l) subject to the condition:

$$\theta_i \in \left[0, \frac{\pi}{2}\right] \Leftrightarrow \sin\theta_l \in \left[0, \frac{R_E}{R_E + h}\right] \, . \qquad (10)$$

The only term in (4) that has not been explicitly expressed as a function of the look angle remains the orthogonal baseline $B_\perp$, which is also the only one that depends on the relative position of the two satellites. It is important to remark that in "across-track" interferometry, $B_\perp$ is not only influenced by the B_{xt} component of the baseline, but also by the B_r component. With reference to the acquisition geometry depicted in the right panel of Fig. 2, the orthogonal baseline can be obtained as:

$$B_\perp(\theta_l, u) = |B(u) \cdot \sin(\alpha - \theta_l)| =$$
$$= |-B_r(u)\sin\theta_l + B_{xt}(u)\cos\theta_l| = \qquad (11)$$
$$= a|\delta e\cos(u - \varphi)\sin\theta_l + (-1)^k\delta i\sin(u - \varphi)\cos\theta_l|,$$

where the last form has been obtained by imposing the condition: $\vartheta = \varphi + k\pi$. The look angle is defined as positive for a right-looking radar.

For given orbital parameters of the formation (a, $\delta e, \delta i, \varphi, \vartheta$), the HoA therefore becomes a function of the two variables u and $\theta_l(s)$ given by (12).

$$\mathrm{HoA}(\theta_l(s), u) =$$
$$\frac{\lambda\left[(R_E+h)\cos\theta_l(s) - \sqrt{(R_E+h)^2\cos^2\theta_l(s) - (h^2 + 2R_E h)}\right]\frac{R_E+h}{R_E}\sin\theta_l(s)}{a|\delta e\cos(u-\varphi)\sin\theta_l(s) + (-1)^k\delta i\sin(u-\varphi)\cos\theta_l(s)|} \, . \qquad (12)$$

IV. OPTIMIZATION PROBLEM

The purpose of the optimization is to minimize the variability of the HoA with respect to a given reference value, $\mathrm{HoA}^\star$. Denoting with $s_A(u)$ and $s_B(u)$ the boundaries of the total ground width to be imaged as functions of the mean argument of latitude, we aim at defining them to minimize the deviation between the HoA and $\mathrm{HoA}^\star$ according to a selected metric. In the following, we will omit making explicit the dependency on u to facilitate readability. Thanks to (8), s_B is known from s_A and the width of the swath, which in turn depends only on the latitude. Formally, we seek the function s_A that minimizes the functional J in the following equation:

$$\arg\min_{s_A} J := \int_{s_A}^{s_A+W_g}(\mathrm{HoA}(s, u) - \mathrm{HoA}^\star)^2\, ds \, . \qquad (13)$$

To find the minimum of J, we evaluate it in correspondence with its stationary points, which satisfy:

$$\frac{\partial}{\partial s_A}\int_{s_A}^{s_A+W_g}(\mathrm{HoA}(s, u) - \mathrm{HoA}^\star)^2\, ds = 0 \, . \qquad (14)$$

The previous equation could be solved with Leibniz's integration rule, provided that the integrand is continuous over the interval $[s_A, s_A + W_g]$. However, this is not guaranteed for every latitude, since beyond a certain u, there is always a value of the look angle, which we will refer to as θ_l^{cr}, for which $B_\perp$ goes to zero, and the HoA reaches an asymptote. This critical angle can be computed by imposing $B_\perp = 0$ in (11):

$$\tan(u - \varphi) = (-1)^{k+1}\frac{\delta e}{\delta i}\tan(\theta_l) \, . \qquad (15)$$

If we fix $\varphi = \pi/2$ and $\vartheta = \varphi + \pi$ (as is the case for TanDEM-X), we ensure that the function in the integral is continuous for $u \in [0, \pi/2)$ because the left and right-hand terms in (15) would always have opposite signs, and $B_\perp$ could nullify only when $u = \pi/2$ and $\theta_l = 0°$ (*i.e.*, at the poles with the radar nadir-pointing). Therefore, (14) can be easily solved for u belonging to the first quadrant.

Please notice that the HoA as given by (12) has a period of π with respect to u; thus, to guarantee global coverage, it is enough to consider half of the points of the orbit. More precisely, we can focus on a single hemisphere, which will be mapped, for example, during the ascending part of the orbit; the opposite hemisphere will then be mapped during the descending part, and the HoA will be the same for each pair $\{\hat{u}, \pi + \hat{u}\}$. Thanks to the polar orbit hypothesis, a value of $\hat{u}$ belonging to a given quadrant uniquely defines a pair of hemisphere-orbit's half: For example, the points where $u \in (0, \pi/2)$ are in the northern hemisphere, imaged in the ascending half of the orbit. This is crucial because it ensures the continuity of the integrand for global coverage. Table I lists the intervals of u where the integrand is continuous depending on the parity of k and the looking direction, for $\varphi = \pi/2$. For a given combination of the look direction and the parity of k, Table I therefore allows determining whether the optimal solution can be found in the Northern or Southern hemisphere using an ascending or descending orbit.

TABLE I
ACQUISITIONS ENSURING CONTINUITY FOR $\varphi = \pi/2, \vartheta = \varphi + k\pi$

Look direction	k	Continuity interval	North hemisphere	South hemisphere
right	odd	$u \in [0, \pi/2) + k\pi$	ascending	descending
	even	$u \in (3\pi/2, \pi] + k\pi$	descending	ascending
left	odd	$u \in (3\pi/2, \pi] + k\pi$	descending	ascending
	even	$u \in [0, \pi/2) + k\pi$	ascending	descending

Applying Leibniz's rule, the solution to (14) is given by one of the following two expressions:

$$\text{HoA}(s_A) = \text{HoA}(s_A + W_g);\qquad(16)$$

$$\frac{\text{HoA}(s_A) + \text{HoA}(s_A + W_g)}{2} = \text{HoA}^\star.\qquad(17)$$

Notably, (16) does not admit a solution in any of the cases reported in Table I. This is because the function $\text{HoA}(s)$ is monotonic with respect to s except when the look angle reaches θ_l^{cr}, which we explicitly avoid. Substituting the expression of the HoA from (12) into (17), we obtain a non-differential scalar problem, which cannot be solved in closed form.

Nevertheless, an analytical solution can still be found by introducing the following two approximations: 1) the slant range is expressed according to the flat-Earth geometry, and 2) the HoA is linear with respect to s:

$$\begin{cases} r_0 \approx \dfrac{h}{\cos\theta_l} \\ \dfrac{\text{HoA}(s_A) + \text{HoA}(s_A + W_g)}{2} \approx \text{HoA}\left(s_A + \dfrac{W_g}{2}\right) \end{cases}\qquad(18)$$

The approximation 2) will be substituted by a more accurate, second-order expression in the following (see eqs. (22)-(24)). The idea is to determine an approximation $\widetilde{\theta_l}$ of the look angle $\theta_l^\star(s^\star)$, solution of $\text{HoA}(\theta_l^\star) = \text{HoA}^\star$, and assume a swath perfectly centered around the corresponding point on the ground: $\tilde{s}$. Inserting (4) in (17) and considering the approximations of (18), we obtain the four-degree polynomial

$$t^4 - 2(-1)^k \left(\frac{\delta e}{\delta i \tan(u-\varphi)} + (-1)^j \frac{\lambda}{\text{HoA}^\star} \frac{R_E + h}{R_E} \frac{h}{\delta i \sin(u-\varphi)}\right) t^3 - 2t^2$$
$$+ 2(-1)^k \left(\frac{\delta e}{\delta i \tan(u-\varphi)}\right.$$
$$\left. - (-1)^j \frac{\lambda}{\text{HoA}^\star} \frac{R_E + h}{R_E} \frac{h}{\delta i \sin(u-\varphi)}\right) t + 1 = 0,\qquad(19)$$

where

$$t = \tan(\widetilde{\theta_l}/2),\qquad(20)$$

and j is even or odd, if the argument of the absolute value in (11) is positive or negative, respectively. Among the (at most) four real roots of eq. (19), the relevant one is the positive one that lies within incidence angle range corresponding to the maximum (equatorial) access range.

Although reasonable, the approximations in (18) introduce an error that shifts the resulting swath away from the nadir compared to the exact one. To compensate for it, we propose the following corrections to be applied ex-post, i.e., once (19) has been solved. First, we consider that the first assumption underestimates the actual value of the slant range, leading to an overestimation of the angle $\theta_l^\star$. Since the introduced error is relatively small, a first-order correction is sufficient to correct it. Specifically, this consists of performing a single step of the Newton method:

$$\theta_l^\star \approx \widetilde{\theta_l} + \frac{\text{HoA}^\star - \text{HoA}(\widetilde{\theta_l})}{\frac{\partial \text{HoA}}{\partial \theta_l}\big|_{\widetilde{\theta_l}}}.\qquad(21)$$

The linear hypothesis, on the other hand, assumes that the point $\tilde{s}$ to be kept at the center of the swath to respect (17) coincides with $s^\star$. This introduces an error that depends on how much the function $\text{HoA}(s)$ differs from a straight line. To compute the shift between $\tilde{s}$ and $s^\star$, it is therefore necessary to consider the non-linear behavior of $\text{HoA}(s)$, which we account for by substituting its Taylor expansion truncated to the second order into (17). The required derivatives of the HoA with respect to s can be computed with the chain rule:

$$\text{HoA}' = \frac{\partial \text{HoA}}{\partial s} = \frac{\partial \text{HoA}}{\partial \theta_l} \frac{d\theta_l}{ds};\qquad(22)$$

$$\text{HoA}'' = \frac{\partial^2 \text{HoA}}{\partial s^2} = \frac{\partial^2 \text{HoA}}{\partial \theta_l^2}\left(\frac{d\theta_l}{ds}\right)^2 + \frac{\partial \text{HoA}}{\partial \theta_l}\frac{d^2\theta_l}{ds^2},\qquad(23)$$

where the expressions of all factors are obtainable leveraging (7) and (12). The shift between the two points therefore reads:

$$\delta = \tilde{s} - s^\star = -\frac{\text{HoA}'(s^\star)}{\text{HoA}''(s^\star)} + \sqrt{\left(\frac{\text{HoA}'(s^\star)}{\text{HoA}''(s^\star)}\right)^2 - \frac{W_g^2}{4}}.\qquad(24)$$

V. TanDEM-X Examples

Some examples of the proposed method's application are presented below, using the TanDEM-X mission as a reference. The two distinct scenarios reported in Table II are considered: In the first one, the orbital parameters are taken from [4]; in the second one, we set the parameters $\delta e = \delta i$ as used by TanDEM-X to map high latitudes, as described in [5].

Fig. 3 illustrates how the optimization process influences the HoA across the swath for various latitude values, without limitations on the access range, in scenario 1. It is clear that the proposed solution progressively introduces a shift towards the nadir, keeping the HoA centered around the desired value as the latitude increases.

In practice, the radar would select an increasingly smaller part of the ground access range initially covered at the equator when approaching the poles, i.e., it is here assumed that the optimal swath must never exceed the limits imposed at the equator (this can be justified, e.g., by radar observation requirements). The result of the optimization with and without the equatorial boundaries is reported in Fig. 3 (a), with both the numerical and the analytical, approximated solution. The

TABLE II
TanDEM-X PARAMETERS IN TWO DISTINCT MISSION PHASES

	$a\delta e$	$a\delta i$	φ	ϑ	$\text{HoA}^\star$	W_{g0}
Scenario 1	300 m	600 m	$\pi/2$	$3\pi/2$	30 m	240 km
Scenario 2	500 m	500 m				

maximum error between the two is 0.37 km, or 0.15% of the access range for the quadratic approximation. Remarkably, the correction factors play a crucial role, as the solution of (19) would result in an error of 20.27 km, equal to 8.45% of the access interval for the linear approximation.

Focusing on scenario 1, the shape in Fig. 3 (b) shows that the optimal look angle increases to a maximum and then decreases with the latitude. This behavior is mainly due to the orthogonal baseline, which increases in the first part of the orbit, reaching its maximum when

$$\tan u = \pi/2 + \frac{\delta e}{\delta i} \tan \theta_l, \tag{25}$$

and then decrease, as the satellites move towards the pole. For $\varphi = \pi/2$ or $3\pi/2$, the influence of δe and δi is well separable: They respectively determine the HoA at the poles ($u = \pi/2$) and at the equator ($u = 0$):

$$\text{HoA}|_{u=\pi/2} = \frac{\lambda r(\theta_l)}{a \delta e} \frac{R_E + h}{R_E} ; \tag{26}$$

$$\text{HoA}|_{u=0} = \frac{\lambda r(\theta_l)}{a \delta i} \frac{R_E + h}{R_E} \tan(\theta_l). \tag{27}$$

This is a direct consequence of having chosen $\varphi = \pi/2$, for which the separation between satellites is exclusively in the across-track direction at the equator and in the vertical direction at the poles, as in TanDEM-X. Remarkably, these last two equations explain the optimal swath in Fig. 3 (b) to move towards the nadir as the latitude increases. In fact, to keep a constant HoA, we must have:

$$\frac{r(\theta_l)|_{u=\pi/2}}{\delta e} = \frac{r(\theta_l)\tan(\theta_l)|_{u=0}}{\delta i}, \tag{28}$$

from which it follows that $\theta_l|_{u=\pi/2} < \theta_l|_{u=0}$ (*i.e.*, the ideal swath is closer to the nadir at the poles than at the equator) when:

$$\frac{r(\theta_l)|_{u=\pi/2}}{r(\theta_l)|_{u=0}} < 1 \Leftrightarrow \tan(\theta_l) < \frac{\delta i}{\delta e}. \tag{29}$$

Since the nominal parameters reported in Table II are such that $\delta i = 2\delta e$, the last equation becomes:

$$\theta_l < \arctan(2) \approx 63.4°, \tag{30}$$

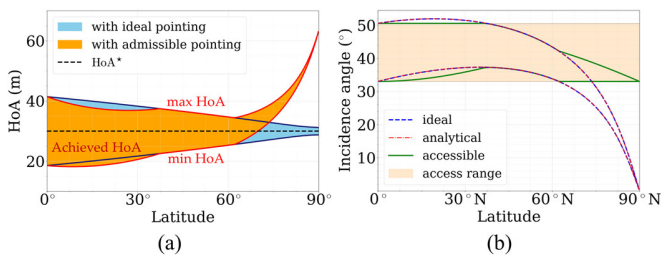which is likely to be verified in realistic scenarios.

Fig 3. Optimal solution for scenario 1 in Table II. (a) HoA achieved at different latitudes; the ideal HoA (blue) is centered around the target value of 30m. (b) Ideal and accessible swaths; the numerical and analytical solution are represented in blue and red, respectively.

TABLE III
RMSE FOR SUB-OPTIMAL VS. OPTIMAL STRATEGIES

Strategy	RMSE with respect to HoA* = 30 m			
	Scenario 1		Scenario 2	
Near range acquisition	6.12 m	20.4%	7.77 m	25.9%
Center of the ground access range	7.06 m	23.5%	6.69 m	22.3%
Optimal incidence angle	5.63 m	18.7%	5.89 m	19.6%

To evaluate the benefit of the proposed strategy, we compare it with two other straightforward cases. In the first case, the swath is always starting at the nearest point within the access range; in the second case, the swath is taken at the center of the access range. In Table III is reported the root mean square error (RMSE) with respect to the target value HoA* = 30 m for all three strategies in the two scenarios listed in Table II.

Notably, the choice of the formation geometry, and specifically of the nominal values of δe and δi profoundly influences the optimal solution. This explains why each of the two straightforward strategies outperforms the other in different scenarios. The poorest performance for these strategies occurs in scenario 2, where the optimal swath coincides with the farthest part of the access range from the radar. Regarding the worst-performing near-range acquisition, the optimized solution achieves an absolute improvement of 1.88 m, corresponding to a relative error reduction of approximately 24%. As for the effects related to the Earth rotation, it has been verified through numerical simulations that, for the case studies considered, the coupling effect between along-track and across-track components is negligible (HoA deviation < 2 %).

VI. CONCLUSIONS

This letter presented an analytical method for selecting the incidence angle in single-pass across-track SAR interferometry using a Helix formation. The proposed solution is the result of a two-step process, in which an initial estimate, obtained by solving a fourth-degree polynomial equation, is refined with the introduction of suitable correction factors. Examples based on TanDEM-X orbit parameters show that the results match almost perfectly those obtained numerically. Ultimately, the proposed strategy offers an improvement in the homogeneity of the height of ambiguity compared to fixed-angle approaches.

VII. REFERENCES

[1] G. Krieger, I. Hajnsek, K. P. Papathanassiou, M. Younis and A. Moreira, "Interferometric synthetic aperture radar (SAR) missions employing formation flying," *Proceedings of the IEEE*, vol. 98, no. 5, pp. 816-843, 2010.
[2] S. D'Amico and O. Montenbruck, "Proximity operations of formation-flying spacecraft using an eccentricity/inclination vector separation," *Journal of Guidance, Control, and Dynamics*; vol 29, 05 2006.
[3] C. Oliver and S. Quegan, "Understanding synthetic aperture radar images," SciTech Publishing, Inc., 2004.
[4] S. D'Amico, O. Montenbruck, C. Arbinger, and H. Fielder, "Formation flying concept for close remote sensing satellites," AIAA Space Flight Mechanics Conference, Advances in the Astronautical Sciences, vol. 120, AAS, 2005, pp. 831-848.
[5] O. Montenbruck, R. Kahle, S. D'Amico, and J.-S. Ardaens, "Navigation and control of the TanDEM-X formation," *Journal of the Astronautical Sciences*, vol. 56, pp. 341-357, 07 2009.